PET/CT imaging evidence of FUS-mediated (18)F-FDG uptake changes in rat brain

Hyungmin Kim
Department of Radiology, Brigham and Women's Hospital, Harvard Medical School, Boston, Massachusetts 02115 and Department of Mechanical Engineering, Korea University, Seoul 136-713, South Korea

Mi-Ae Park, Shuyan Wang, Alan Chiu, and Krisztina Fischer
Department of Radiology, Brigham and Women's Hospital, Harvard Medical School, Boston, Massachusetts 02115

Seung-Schik Yoo[a)]
Department of Radiology, Brigham and Women's Hospital, Harvard Medical School, Boston, Massachusetts 02115 and School of Nano Bio Chemical Engineering, Ulsan National Institute of Science and Technology, Ulsan 689-798, South Korea

(Received 28 July 2012; revised 14 January 2013; accepted for publication 15 January 2013; published 12 February 2013)

Purpose: Transcranial focused ultrasound (FUS) delivers highly focused acoustic energy to a small region of the brain in a noninvasive manner. Recent studies have revealed that FUS, which is administered either in pulsed or continuous waves, can elicit or suppress neural tissue excitability. This neuromodulatory property of FUS has been demonstrated *via* direct motion detection, electrophysiological recordings, functional magnetic resonance imaging (fMRI), confocal imaging, and microdialysis sampling of neurotransmitters. This study presents new evidence of local increase in glucose metabolism induced by FUS to the rat brain using FDG (18-fludeoxyglucose) positron emission tomography (PET).
Methods: Sprague–Dawley rats underwent sonication to a unilateral hemispheric area of the brain prior to PET scan. The pulsed sonication (350 kHz, tone burst duration of 0.5 ms, pulse repetition frequency of 1 kHz, and duration of 300 ms) was applied in 2 s intervals for 40 min immediately after the FDG injection *via* tail vein. Subsequently, the PET was acquired in dynamic list-mode to image FDG activity for an hour, and reconstructed into a single volume representing standardized uptake value (SUV). The raw SUV as well as its asymmetry index (AI) were measured from five different volume-of-interests (VOIs) of the brain for both hemispheres, and compared between sonicated and unsonicated groups.
Results: Statistically significant hemispheric changes in SUV were observed only at the center of sonication focus within the FUS group [paired t-test; $t(7) = 3.57$, $p < 0.05$]. There were no significant hemispheric differences in SUV within the control group in any of the VOIs. A statistically significant elevation in AI (t-test; $t(7) = 3.40$, $p < 0.05$) was observed at the center of sonication focus ($7.9 \pm 2.5\%$, the deviations are in standard error) among the FUS group when compared to the control group ($-0.8 \pm 1.2\%$).
Conclusions: Spatially distinct increases in the glucose metabolic activity in the rat brain is present only at the center of sonication focus, suggesting localized functional neuromodulation mediated by the sonication. © *2013 American Association of Physicists in Medicine*. [http://dx.doi.org/10.1118/1.4789916]

Key words: focused ultrasound, sonication, neuromodulation, positron emission tomography

I. INTRODUCTION

Apart from wide usage as a diagnostic imaging modality, ultrasound (US) has been gaining momentum as a therapeutic tool. In particular, focused ultrasound (FUS) has various therapeutic potentials due to its ability to deliver highly focused acoustic energy to a small tissue area without damaging its surroundings by concentrating the acoustic waves on a specific region.[1] Focused acoustic energy, typically given at high intensities (>600 W/cm^2), can noninvasively ablate tissue in a specific location.[2] Therefore, FUS ablation therapy has been applied to the treatment of many types of soft tissue tumors, including tumors in the liver, breast, uterus, prostate, and pancreas, often under the guidance of radiological imaging techniques, such as magnetic resonance imaging (MRI) (Ref. 3) or US.[4]

The sonication of the brain, on the other hand, presents a new set of technical challenges compared to soft tissue sonication, since the skull acts as a sound absorber as well as a reflector of the acoustic beam path.[5] With the advent of multiarray FUS transducer designs, the delivery of FUS through the skull became feasible by controlling the phases of acoustic

waves originating from multiple ultrasound sources surrounding the skull structure. In addition, acoustic frequencies, typically lower than 1 MHz (cf., 2–18 MHz is used for diagnostic imaging), are employed due to the reduced degrees of acoustic attenuation and distortions.[6] The introduction of transcranial FUS opened other neurotherapeutic avenues, such as the treatment of brain tumors or functional neurosurgery *via* thermal ablation,[7,8] and selective drug delivery *via* blood-brain-barrier (BBB) disruption.[9] It is anticipated that these techniques will provide a noninvasive alternative to surgical treatment or radiation/chemo therapy of the brain.

Recently, our group and others have demonstrated that FUS given in pulsed mode at low acoustic intensity (<3 W/cm^2 in spatial-peak temporal-average intensity; I_{spta}) is capable of inducing differential neuromodulatory effects, both excitatory and inhibitory, on the animal brain.[10,11] Unlike existing noninvasive neuromodulatory techniques, such as transcranial direct current stimulation (tDCS) and transcranial magnetic stimulation (TMS),[12] FUS has superior spatial specificity and the ability to penetrate deep into the brain.[1] Therefore, it opens rousing new possibilities for potential therapeutic intervention or, at the very least, could potentially be used as a diagnostic tool to assess region-specific brain function.

The neuromodulatory effects of FUS have been demonstrated *via* direct motion detection by motion sensitive sensor,[13] electrophysiological recordings such as visual evoked potential (VEP) (Ref. 10) or electromyography (EMG) (Ref. 11) stemming from the brain stimulation, and detection of changes in cortical blood-oxygenation level *via* functional MRI (fMRI).[10] Confocal imaging of the ion channel function of the central nervous system (CNS) neurons revealed that Na^+/Ca^{2+} channel activity was altered when the neural tissue were exposed to the pulsed insonication of ultrasound.[14] Indirect evidence of the FUS-mediated functional modulation was also shown by the direct measurement of the extracellular level of neurotransmitters *via* microdialysis techniques.[15,16] These studies provided strong evidence of functional changes in the CNS tissue; however, as to our knowledge, the presence of metabolic changes induced by neuromodulatory FUS has not been thoroughly studied.

In this study, we investigated the feasibility of showing evidence that low-intensity and low-frequency focused ultrasound can modulate the localized brain metabolic activity in a rodent model utilizing 2-deoxy-2-[^{18}F]fluoro-D-glucose (FDG) positron emission tomography (PET). We hypothesized that FUS-mediated functional changes in neural activity alter the regional glucose metabolism of the brain,[17] in turn affecting FDG uptake which can be characterized by FDG-PET imaging.

II. MATERIALS AND METHODS

II.A. Animal preparation

All experiments were conducted under institutional review and approval by the Harvard Medical Area Standing Committee on Animals. Male Sprague–Dawley rats ($n = 17$, 284 $\pm$ 20 g) were used in this study. The animals were deprived of food but allowed access to water for 16–19 h prior to the PET scan. All animals were anesthetized with isoflurane (3.5% for induction, and 1.5% for maintenance, all in 95% oxygen at a flow rate of 1 L/min *via* a nose cone) at 20 $\pm$ 6.5 min prior to the FDG injection.

The first two animals were used for estimating the temporal dynamics of baseline FDG uptake in the absence of sonication (see the section *Determining Timing Windows for Sonication and FDG-PET Scanning* below). One rat was excluded from the study due to abnormal brain anatomy (partial agenesis), which was confirmed by both CT imaging and tissue extraction afterwards. Two groups ($n = 7$ for each) of animals were subjected to the subsequent PET imaging. The experimental group, denoted as "FUSg," underwent sonication, whereas the control group, denoted as "CTLg," was not exposed to sonication, but otherwise underwent conditions that mimicked all other experimental features of the FUSg, including the application of the sonication setup and scan protocols. The weight of the animals in each group (279 $\pm$ 15 g for FUSg, 281 $\pm$ 20 g for CTLg) was balanced (t-test; $t(7) = 0.27$, $p > 0.05$). A 24-gauge catheter was inserted in the rat's tail vein prior to applying the sonication setup and flushed with a mixture of saline and heparin to maintain patency. The application of the catheter was necessary to deter further movement of the animals during the injection of the FDG and to control the injection time.

II.B. Sonication setup

After catheterization, the rats were placed on a MRI-compatible stereotactic frame (SRP-AR, Narishige, Japan) that demobilized the head for sonication. The schematics of the sonication setup is shown in Fig. 1(a). The sonication was targeted near the thalamic area unilaterally using the optical laser guidance procedure described in our previous study.[16] The side of sonication was randomized and balanced across the animals ($n = 3$ for left hemisphere, $n = 4$ for right hemisphere for FUS group). Two laser spots were initially coincided on the rat's scalp with respect to external anatomical landmarks (e.g., midline between eye and ear lines, ~3 mm

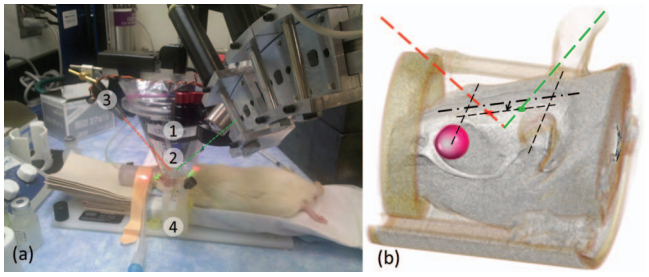

FIG. 1. (a) FUS experimental setup: (1) a single-element FUS transducer, (2) a plastic bag containing degassed water to couple the sonication path to the scalp, (3) laser pointers, and (4) a MRI-compatible stereotactic frame. (b) Illustration of the sonication guidance, where the distance between the laser dots on the scalp (7.4 mm) determined the sonication depth. The arrow indicates the ~3 mm offset distance and direction (left thalamus in the presented case).

offsetting the midsagittal line). The transducer was lowered to the scalp, while the depth of the sonication was subsequently estimated based on the distance between the lasers based on geometrical relationship with respect to the transducer [as illustrated in Fig. 1(b)].

II.C. FUS transducer

An air-backed, spherical segment FUS transducer (6 cm in diameter, 7 cm in radius of curvature, 350 kHz of fundamental frequency) was used. The acoustic pressure field was calibrated in rubber-laid degassed water tank using a needle-type hydrophone (HNR500; Onda, Sunnyvale, CA) mounted to the 3-axis robotic platform (Bi-Slides; Velmex, Bloomfield, NY). First, the focal plane was determined by the time-of-flight information of ultrasound while monitoring with oscilloscope (DSO-X 2012A, Agilent Technologies, Santa Clara, CA). The acoustic field was then mapped in space covering 2.5×2.5 cm^2 with 0.5 mm steps in the transversal direction, and 7×3 cm^2 with 1 mm steps in the longitudinal direction along the sonication path. The spatial-peak pulse-averaged intensity (I_{sppa}) was estimated by integrating the pulse intensity at its spatial maximum and dividing it by the pulse duration according to the American Institute of Ultrasound Medicine (AIUM) standards.[18] The spatial-peak temporal-average intensity (I_{spta}) was calculated by multiplying the duty cycle of the pulse operation to the I_{sppa}. The geometry of the acoustic focus was roughly cigar-shaped (6.5 mm in diameter, 24 mm in length), and was estimated from the contour exceeding the full-width-at-half maximum (FWHM) of the acoustic intensity [Figs. 2(a) and 2(b)].

II.D. Sonication parameters

Two serially connected waveform generators (33210A, Agilent, Santa Clara, CA) generated specific pulsed waves; pulse-repetition frequency (PRF) of 1 kHz, tone-burst duration (TBD) of 0.5 ms, sonication duration (SD) of 300 ms, and sonication intervals of 2 s. The generated waveforms were amplified by a linear power amplifier (240L, ENI Inc., Rochester, NY), which has 50 dB nominal power gain, and transmitted to the ceramic ultrasound transducer (Channel Tech group, CA).

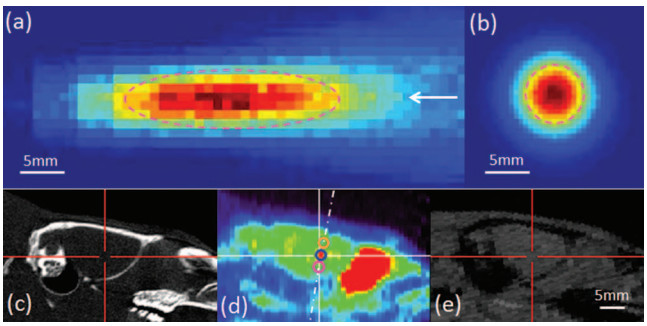

FIG. 2. Acoustic intensity profile of 350 kHz FUS transducer in (a) longitudinal and (b) transversal plane of sonication. The arrow indicates the direction of sonication. At FWHM of the acoustic intensity, cigar-shaped (6.5 mm in diameter and 24 mm in length) acoustic focus is depicted in dash line. An example of coregistered images: (c) CT, (d) PET, and (e) MRI. The crosshairs indicate the corresponding expected acoustic focus on each modality. The dashed-dotted line indicates the approximated sonication path. The circles along the dashed-dotted line in (d) depict the VOIs defined inside the acoustic focus (cen.focus: top, sup.focus: middle, inf.focus: bottom, 2 mm in diameter). The bars indicate 5 mm.

The degree of pressure attenuation through the rat skull in 350 kHz was measured from freshly isolated *ex vivo* rat skulls ($n = 5$). For each rat skull, the pressure attenuations were measured three times (the ratio of acoustic pressure measured in the presence and absence of the rat skull), and averaged. The averaged pressure attenuation across the five rat skulls was calculated to be $12.1 \pm 2.3\%$ (s.d.). Considering the pressure attenuation, the resulting acoustic intensity was set to be 3 W/cm^2 in I_{spta}. The corresponding mechanical index (MI) was 0.74, where peak negative pressure was 0.43 MPa.

The sonication parameters (0.5 ms TBD, 1 kHz PRF, 300 ms SD) used in this study were recently reported to elicit tail movement in rats by sonicating on the motor cortex.[13] The difference between the previous work and the present study is that the lower acoustic intensity (3 W/cm^2 I_{spta}) was adopted (4.5 W/cm^2 I_{spta} was used in the previous study[13]) to comply with the upper limit of ultrasound physiotherapy equipment set by the International Electrotechnical Commission (IEC) standard.[19]

To confirm the excitatory effect of the prescribed sonication parameters used in this study, additional experiments were conducted to determine the threshold for acoustic intensity that elicits motor function in rats ($n = 9$, weight $= 277 \pm 21$ g) under anesthesia (intraperitoneal injection of ketamine/xylazine mixture at 80:10 mg/kg). The sonication, using the same pulsing parameters as the PET imaging (i.e., 0.5 ms TBD, 100 Hz PRF, 300 msc SD), was transcranially administered to the rat's tail motor area of the brain,[20] and the acoustic intensity which elicited tail movement, indicating successful neural excitation,[11,21] was measured using the method described in our previous work.[13] Tail movement was detected at acoustic intensities above 3.1 ± 0.6 W/cm^2 I_{spta} across the animals tested. Based on the investigation by Tufail and co-workers[11] which examined the relationship between acoustic frequency and intensity on cortical excitation by pulsed ultrasound, acoustic intensities lower than the threshold also reliably activate the descending corticospinal circuits. Therefore, it is highly suggestive that the acoustic intensity of 3 W/cm^2 I_{spta} elicits successful neural excitation for the PET imaging.

II.E. FDG-PET/CT and magnetic resonance (MR) imaging

PET/CT imaging was performed using a commercial μPET/CT scanner (eXplore Vista, GE healthcare). The detector consisted of two types of crystals, lutetium-yttrium oxyorthosilicate (LYSO) and gadolinium oxyorthosilicate (GSO), which were utilized for depth-of-interaction information for an improved resolution based on different scintillation decay time.[22] The spatial resolution was 1.6 mm at the center of the field-of-view (FOV), which was determined by FWHM

of Gaussian function, and yielded ~4% count sensitivity at the energy window of 250–700 keV. The data were acquired in 3D, and reconstructed using Fourier rebinning (FORE) and conventional ordered-subsets expectation-maximization (OSEM) algorithm with 16 subsets and 2 iterations.[23]

PET images were reconstructed to generate 61 tomographic images of 175 × 175 in matrix size that spanned the 68 × 68 mm in the FOV. The voxel dimensions of the reconstructed images were 0.39 × 0.39 × 0.78 mm^3. CT images were then reconstructed to provide 432 slices of 520 × 520 in matrix size, 63 × 63 mm in FOV, 0.12 mm in slice thickness, which resulted in isotropic voxel (0.12 × 0.12 × 0.12 mm^3). PET images were corrected for random and scatter coincidence events, while the CT information was used for attenuation correction, during the reconstruction.

After PET/CT scans, the follow-up MRI scans were performed on selected animals ($n = 3$) to provide additional soft-tissue related anatomical information to confirm the location of the regions representing localized higher FDG-uptake, rather than providing the data for the biological safety due to sonication. The animals were anesthetized with an intraperitoneal injection of 80 mg/kg ketamine and 10 mg/kg xylazine prior to scanning. The anatomical MR images were acquired using spoiled gradient recalled (SPGR) sequence (TR/TE = 11.2/4.05, flip angle = 12°, matrix = 512 × 512, FOV = 14 cm, slice thickness = 1 mm, number of slices = 113), and used to validate the anatomical location of the volume-of-interest (VOI). By manual positioning (translation and rotation) based on the anatomical information (e.g., cranium boundary), MR images were initially aligned to CT images, which was used for the initial condition of the subsequent automated volumetric registration method in order to increase registration accuracy and speed. Refined registration was subsequently performed using automatic registration method based on normalized mutual information.[24] Since CT images contained the same amount of relevant anatomical information as MR images, while sharing the same coordinate system definition of PET, we did not perform additional registration of MR images to PET images. An example of coregistered images is demonstrated in Fig. 2.

II.F. Determining timing windows for sonication and FDG-PET scanning

Since PET is not inherently a sensitive imaging modality, it requires multiple data acquisition to increase signal-to-noise ratio (SNR). In addition, FDG uptake over time is highly dependent on the organs and species.[25] Therefore, the determination of the scan period is crucial in successful PET imaging. To determine the baseline FDG uptake curve over time for a rat brain, two rats underwent dynamic PET scans without sonication for 2 h, and temporal analysis was performed to evaluate the dynamics of FDG uptake after the FDG injection (14.4 MBq) as shown in Fig. 3. This provided the information for determining the sonication and PET scan timing. PET data were acquired in list-mode.[26] The 2-h list-mode data was reconstructed into 12 volumes with standardized uptake value (SUV) in 10 min intervals. Then, a spherical VOI with a 10 mm-diameter was drawn near the thalamus and the average SUV values were calculated over time.

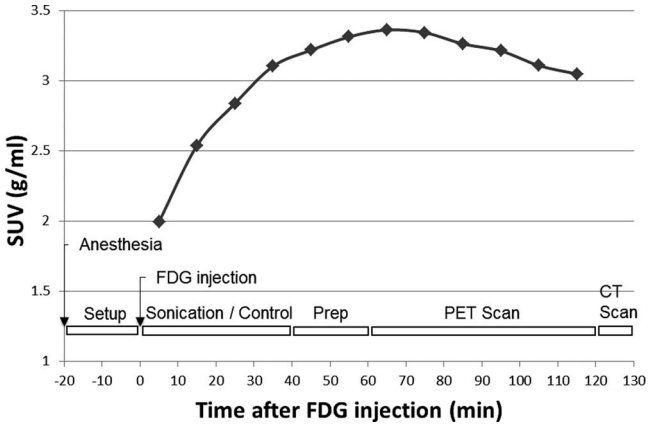

FIG. 3. The averaged temporal dynamics of FDG uptake in rats without any sonication (the dotted plot, $n = 2$), and the timeline of the experimental procedures (as illustrated at the bottom): zero value was set to FDG injection timing. "Setup" includes catheter placement for FDG injection and sonication setup procedures. "Prep" represents the preparations for PET/CT scanning (rat positioning in the scanner, placement of probes for physiological monitoring, scout image scanning).

II.G. Experiment protocols for group comparison

Based on the findings from the temporal dynamics of the unsonicated rats (Fig. 3), the FDG uptake reached its plateau at about 60 min after the FDG injection. Since we intended to sonicate the animals during the uptake period of FDG in the brain, the sonication was given immediately after the FDG injection (14.65 ± 0.79 MBq for FUSg, 14.42 ± 1.79 MBq for CTLg). The injected dose was statistically equivalent in both groups [t-test; $t(7) = 0.30$, $p > 0.05$].

A detailed timeline of the experimental procedures including anesthesia, FDG injection, sonication, and PET/CT scans is depicted in Fig. 3. For the catheterization and the target planning for sonication, the rats were under isoflurane for about 20 min prior to FDG injection (−23 ± 2.6 min for FUS group, −17 ± 6.7 min for CTL group), and balanced for both groups [t-test; $t(7) = 1.90$, $p > 0.05$]. A wash-out effect dominated and diminished the amount of gamma ray detected by the scanner, 60 min after the FDG injection. We maximized the time duration for the sonication exposure within the FDG uptake period (the first 60 min after the FDG injection). Since about 20 min of preparation time was needed for subsequent PET scanning (including transporting animal from preparation table to scan table, placing electrodes for physiological monitoring, and scanning scout image for determining field-of-view), the sonication was initiated immediately after the FDG injection and continued for 40 min. Animals were sonicated for 40 min to allow for sufficient preparation time for the initiation of the PET scan (20 min) while maximizing the chances of detecting FUS-mediated changes in the FDG-uptake period. For the FUS group, a CT-visible bead was placed on the nose cone to mark the side of sonication. Then, the scout CT image was acquired to

include the entire brain in the FOV for the subsequent PET/CT scans. The dynamic PET scan was subsequently performed in list-mode for 60 min. During the PET scanning, heart rate and rectal body temperature were measured every 5 min using electrocardiogram and a thermistor, respectively. At the end of the PET scan, CT images were acquired to supply anatomical references and attenuation corrections. The rats were transferred to a shielding container for radioactive decay to reach safe levels (for 10 half-lives; one half life is 110 min) before they were transferred back to the animal facility.

II.H. Data analysis

The localized changes in glucose metabolism, as induced by the application of the FUS, were evaluated. To assess for the group-level metabolic activity across the animal, we analyzed the SUV value from the specific volumes-of-interest in the brain. Atlas-based group analysis technique, which requires anatomical normalization to standardized spatial coordinates,[27,28] could not be used since the side of the sonication was alternated and minor inconsistencies (varying ~2 mm) in positioning the sonication focus were present (the extent of spatial errors are discussed in Ref. 13).

Ten spherical VOIs (diameter 2 mm) were defined to measure the SUV signals from the different regions of the brain, i.e., frontal lobe, center of acoustic focus, cerebellum, and superior and inferior to the center of acoustic focus from both hemispheres. The VOIs located superior and inferior to the sonication center were drawn along the sonication path (normal to the skull surface), adjacent to the VOI (without any gap inbetween) indicating the center of sonication focus as depicted in Fig. 2(d). The greater VOI was not used for obtaining the SUV due to the partial volume effects and subsequent reduction of the SUV signal.[29] For example, the VOIs covering the whole hemisphere did not show any statistically significant hemispheric differences in SUV for either the FUS group [paired t-test; $t(7) = 0.87$, $p > 0.05$] or CTL group [paired t-test; $t(7) = 0.70$, $p > 0.05$]. The size of the VOI was determined to approximate the actual spatial profile of the increased metabolic activity at the sonication locus in the transverse plane. In localizing the VOIs around the sonication center, higher metabolic activity present in the Harderian gland, cerebellum, and middle of the brain was regarded as background metabolic activity regardless of sonication. This was justified by the fact that the similar patterns and amount of activity are also detected in the control scans [Fig. 4(c)] and in the previous study.[30] The focal VOI was chosen based on the coordinates of the sonication target location given by the optical guidance.[16] The additional VOIs superior and inferior to the sonication center were defined along the estimated sonication path [see Fig. 2(d)]. Then, the SUV statistics inside the VOIs were measured using the open-source image analysis software (AMIDE, http://amide.sourceforge.net).[31]

The average SUVs were calculated at 1 h postinjection according to the formula: SUV = c/(D/W), where c was the activity concentration within the VOI in the brain (Bq/ml), D was the injected dose (Bq), and W was the rat's body weight (g). For comparison within the group, paired t-test was performed on the averaged SUV of each VOI. In addition, for intergroup comparison, unpaired t-test was performed on asymmetry index (AI),[32] which was defined by $(SUV_{FUS} - SUV_{CTL})/[(SUV_{FUS} + SUV_{CTL})/2] \times 100$ for FUS group $(SUV_{RIGHT} - SUV_{LEFT})/[(SUV_{RIGHT} + SUV_{LEFT})/2] \times 100$ for CTL group. An AI of zero indicates there is no hemispheric difference in SUV, while a positive value indicates higher FDG uptake on the sonicated side.

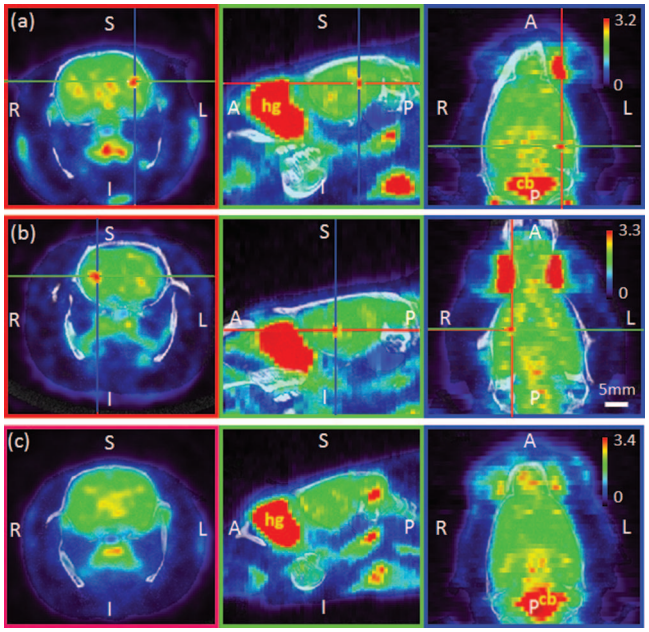

FIG. 4. Examples of PET/CT images: Sonication was given on the left (a) or right (b) hemisphere, whereas (c) shows the images from the control condition (i.e., no sonication). The crosshairs in (a) and (b) indicate the location of the center of the acoustic focus. Coronal (first column)/sagittal (second column)/transversal (third column) planes. The vertical bar in the transversal plane indicates pseudocoloring scale of the SUV range. The orientation notations represent the anatomical directions (A: anterior, P: posterior, S: superior, I: inferior, R: right, L: left). Apart from the sonication site, the Harderian gland (hg) and cerebellum (cb) showed relatively higher FDG uptake. The horizontal bar indicates the mm scale, which applies to all images.

II.I. Histological assessment

In order to investigate the safety of the applied sonication, histological analysis was performed on the selected animals ($n = 2$), which were allowed to survive for 36 days after the experiment. The skull was surgically extracted and fixed by systemic circulation of formalin (10%) immediately after sacrificing the animal, and the skull was extracted. The extracted skulls were immersed in 10% formalin solution for an additional one to two weeks before extracting brain tissue for sectioning. Serial sections were applied perpendicular to the sonication path from brain cortex, hippocampus, and thalamus, and histological analysis using hematoxylin and eosin (H&E) stain was then performed to examine the presence of hemorrhaging or tissue damage.

III. RESULTS

III.A. FDG-PET/CT imaging

The averaged heart rate (248 ± 16 bpm for FUSg, 251 ± 38 bpm for CTLg) and the averaged rectal body temperature (35.7 ± 0.9 °C for FUSg, 35.9 ± 1.1 °C for CTLg) were indifferent between the two groups [t-test; $t(7) = 0.20$, $p > 0.05$ for heart rate; $t(7) = 0.35$, $p > 0.05$ for rectal body temperature].

In Fig. 4, the fused images of PET/CT of the rat are shown. In the first and second rows, representative images of the rats, which received sonication on each side of the brain hemisphere (left and right; the sonication target is indicated by the crosshair), are shown. An example of the PET image acquired from an unsonicated rat is displayed in the third row. Pseudocoloring was applied to reconstructed SUV volume images (scale is displayed on the right side with absolute SUV range). As pixel values in the SUV images are typically subjected to a large degree of subject-dependent variability, as much as 50%,[33] different color-range schemes for each animal were used to accentuate the isolated SUV uptake patterns in the PET imaging. The location showing increased FDG uptake compared to the contralateral side was closely approximated to the center of sonication focus (<2 mm in diameter) in the sonicated rats, whereas, asymmetric FDG uptake pattern was not observed in the unsonicated rat. It is also notable that, across all animals (sonicated and control), there was higher FDG uptake observed in the Harderian gland (nearby the ocular muscles) and cerebellum relative to other parts of the brain, denoted as "hg" and "cb," respectively. The relatively large FDG uptake in these areas is in good agreement with previous studies.[30,34,35]

For the examination of the spatial variations among defined focal VOIs, the additional analysis was performed. The PET data obtained from FUSg were divided further into two groups with respect to the side of sonication (left: $n = 3$, right: $n = 4$). For each group, the averaged SUV volume data were coregistered to each other using an automated volumetric image registration method based on mutual information.[24] The initial alignment between the volume data was manually performed prior to the automated registration process. Once all the SUV volumes are coregistered, the spatial variation among the location of VOIs was estimated by calculating the distance between the center of each VOI and the centroid (center-of-mass) among the VOIs. The calculation was done separately for each hemisphere. The mean difference was 2.5 mm (standard error = 0.66 mm, $n = 7$), which was close to the error bound previously reported using the optical guidance technique.[16]

III.B. SUV statistics for within-group comparison

In Fig. 5, each paired columns show the SUV measurements on FUS/CTL sides [for FUS group—Fig. 5(a)], or right/left sides [for CTL group—Fig. 5(b)], respectively, for each anatomical regions. For the FUS group, the SUV measurements (FUS/CTL sides) with associated standard errors for each anatomical regions were as follows: 2.19 ± 0.28/2.24 ± 0.29 g/ml for the frontal lobe, 2.68 ± 0.36/2.49 ± 0.36 g/ml for the center of the acoustic focus, 3.87 ± 0.48/3.82 ± 0.42 g/ml for the cerebellum, 2.13 ± 0.26/2.20 ± 0.28 g/ml for the superior side to the center of the acoustic focus, 2.40 ± 0.38/2.31 ± 0.35 g/ml for the inferior side to the center of the acoustic focus. For the CTL group, the SUV measurements (right/left sides) for each anatomical areas were as follows: 2.62 ± 0.46/2.57 ± 0.44 g/ml for the frontal lobe, 3.08 ± 0.63/3.12 ± 0.65 g/ml for the center of the acoustic focus, 4.85 ± 0.88/4.98 ± 0.91 g/ml for the cerebellum, 2.43 ± 0.43/2.41 ± 0.42 g/ml for the superior side to the center of the acoustic focus, 2.80 ± 0.55/2.77 ± 0.54 g/ml for the inferior side to the center of the acoustic focus. Statistically significant changes in FDG uptake on the FUS side as compared to the CTL side was observed only at the center of sonication focus within the FUS group [paired t-test; $t(7) = 3.57$, $p < 0.05$]. There were no significant differences between the right and left hemispheres observed within the CTL group

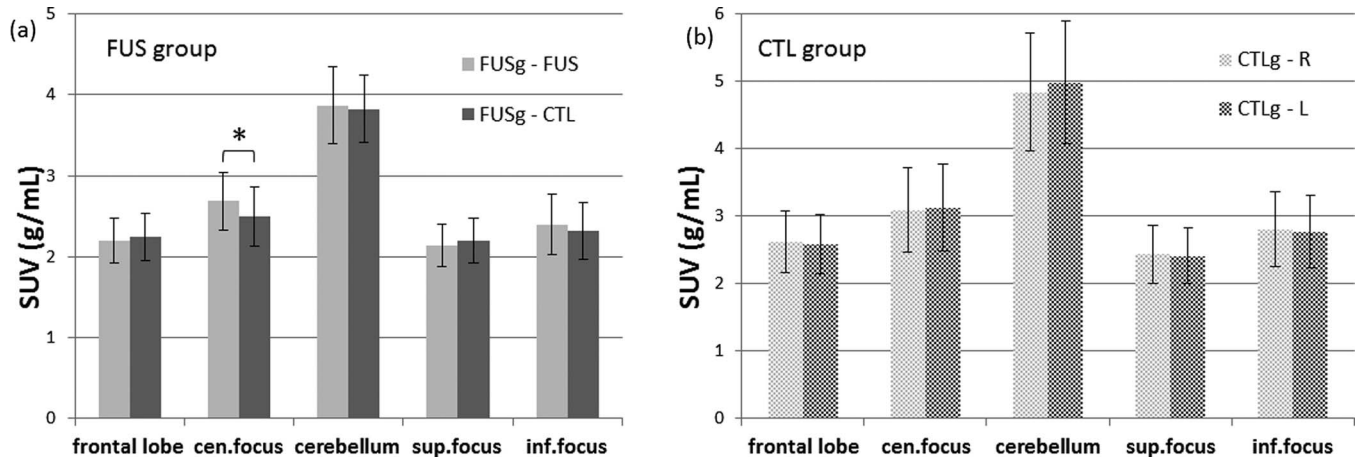

FIG. 5. Comparison in SUV within group: (a) experimental group (FUSg), (b) control group (CTLg). Multiple VOIs were drawn in multiple anatomical regions: frontal lobe, center of acoustic focus (cen.focus), cerebellum, superior to the center of acoustic focus (sup.focus), and inferior to the center of acoustic focus (inf.focus). The asterisk indicates statistically significant differences (paired t-test; $p < 0.05$). The error bars indicate ±1 s.e.m.

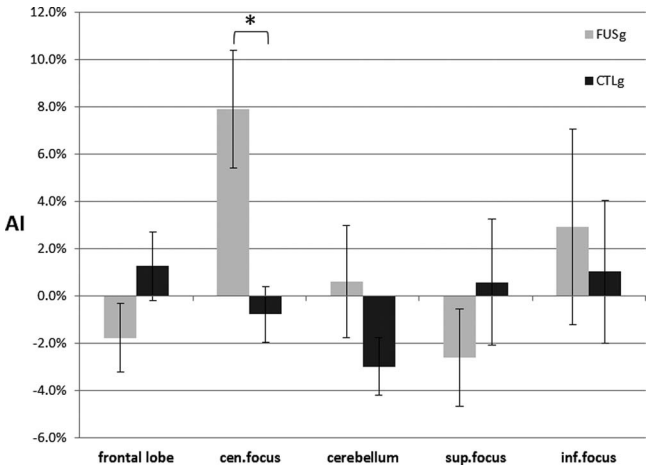

FIG. 6. Comparison in AI between groups (FUSg: experimental group, CTLg: control group, sup.focus: superior to the sonication focus, inf.focus: inferior to the sonication focus). The asterisk indicates the statistically significant differences between groups at sonication focus (t-test; $p < 0.05$). The error bars indicate ± 1 s.e.m.

in any of the VOIs [paired t-test; frontal lobe: $t(7) = 1.59$, $p > 0.05$, cerebellum: $t(7) = 0.44$, $p > 0.05$, superior to sonication center: $t(7) = 1.62$, $p > 0.05$, inferior to sonication center: $t(7) = 0.96$, $p > 0.05$].

III.C. AI statistics for between-groups comparison

In Fig. 6, for each paired columns, the left column indicates the AI of the FUS group, and the right column depicts the AI of the CTL group for each VOI. It is notable that AI obtained from the center of sonication focus is elevated (i.e., $7.9 \pm 2.5\%$ for FUSg, the deviations are in standard error) among the FUS group, compared to the CTL group ($-0.8 \pm 1.2\%$). A statistically significant change in AI was observed at the center of the sonication focus [t-test; $t(7) = 3.40$, $p < 0.05$], where the positive AI indicates the relatively higher FDG uptake on the sonicated area than the unsonicated area. There was no statistically significant difference in AI between groups for the other VOIs [t-test; frontal lobe: $t(7) = 1.60$, $p > 0.05$, cerebellum: $t(7) = 1.46$, $p > 0.05$, superior to sonication center: $t(7) = 1.02$, $p > 0.05$, inferior to sonication center: $t(7) = 0.40$, $p > 0.05$]. The statistical insignificances superior or inferior to sonication center may suggest that the neuromodulatory effect was localized at the center of the focus.

III.D. Postsonication monitoring and histological analysis

During the survival period after the experiment, the behavior of the rats was monitored once every two days until they were sacrificed. None of them exhibited abnormal behavior. Histological analysis did not show the presence of tissue damage or hemorrhage associated with the sonication in any of the animals.

III.E. Justification of sonication parameters

The sonication parameters used in this study were based on the parameters that elicited the tail movement associated with the neural excitation of the motor cortex. On the other hand, suppressive neuromodulation has been observed to occur at a much lower acoustic intensity using a lower duty cycle, i.e., 130 mW/cm^2 I_{spta} (Ref. 36) or 165 mW/cm^2 I_{spta} (Ref. 10) with 5% duty cycle (0.5 ms TBD, 100 Hz PRF).[10,36] All these evidences support that the tested sonication parameters are highly likely to stimulate the neural structures in the sonicated brain area.

IV. DISCUSSION

In this study, pulsed-FUS tailored for excitatory neuromodulation with subsequent small animal FDG-PET scanning demonstrated localized FUS-mediated changes in glucose metabolism of the rat brain. In addition to previously suggested evidences for the neuromodulatory effects of FUS (e.g., motion detection, fMRI, electrophysiological recordings, confocal imaging, and microdialysis of neurotransmitters), this offers further evidence of metabolic changes induced by the neuromodulatory FUS.

Our analysis suggests the confirmation of spatially distinct changes in metabolic activity in the rat brain that coincides with the sonication center. The transcranial sonication increased the glucose metabolic activity at the center of acoustic focus, and resulted in a positive AI value. The control group did not show any significant asymmetry in any of the tested VOIs. The areas of the brain other than the sonication center (i.e., frontal lobe, cerebellum, superior and inferior to sonication center) did not show any significant hemispheric differences in SUV when comparing the sonicated and control groups. One might anticipate the presence of increased metabolic activity in the brain regions other than the sonication center due to neural connectivity.[37,38] However, the data presented in this study suggest that the neuromodulatory effect of FUS is highly localized at the center of sonication focus. The highly localized activation supports the theory of the spatially selective nature of the FUS-mediated neural activation, but may also stem from the lack of detection sensitivity of the FDG-PET. The anesthesia may have also contributed to the dissociation of the brain regions that are activated by the sonication itself.[39,40]

As for the choice of anesthetic agent, isoflurane was preferred over other agents, such as ketamine/xylazine or urethane, since it provides a stable level of anesthesia over the PET study, which requires the data acquisition for more than 2 h. The use of ketamine/xylazine is inadequate for animal PET studies due to its lack of a stable anesthetic level. Urethane, although it provides stable anesthesia over several hours, is only permitted for nonsurvival experiment due to its toxicity.[41] Isoflurane has been used for numerous functional MRI studies on the CNS, covering visual,[42] motor or nonmotor[43,44] circuits. The use of isoflurane confounds but does not eliminate the blood-oxygenation-level-dependent (BOLD) signal responses in these functional MRI studies, which is believed

to be associated with the modification in cerebral vascular function.[45] Rather, isoflurane interferes with "downstream" neural processes in the peripheral nervous system (PNS), which reportedly abolishes motor evoked responses[46] or attenuates the motor evoked potentials (MEP) followed by the motor cortex excitation.[47] This suggests that isoflurane leaves the signs of neuromodulation present in the CNS intact, but may interrupt evoked responses mediated by the PNS. It is congruent to the disappearance of evoked responses made by the FUS stimulation to the brain.[48] These support our justification of using isoflurane as the anesthetic agent in this study to avoid stimulation related movement artifacts while securing sustained level of anesthesia over the duration of the PET scan.

To investigate any potential temperature increase due to the sonication, theoretical temperature elevation was estimated by the formula in the previous study[6,49] (i.e., $\Delta T = 2\alpha It/\rho_b C_p = 2 \times 0.05\ cm^{-1} \times 3\ W\ cm^{-2} \times 0.3\ s/3.796\ J\ cm^{-3}\ ^\circ C^{-1} = 0.02\ ^\circ C$; where α = the absorption coefficient,[50] I = the intensity of ultrasound in the focal region, t = the ultrasound pulse duration, ρ_b = the density of brain tissue,[51] and C_p = the specific heat of the brain tissue[51]). The estimated temperature rise was far below the threshold for any thermal bioeffects. In addition, the temperature changes were not detected in a phantom (detailed method described in Ref. 52) using the same sonication parameters and conditions as the actual experimental setting. However, the presence of possible small hot spots due to reverberation other than the measured spots[53] cannot be completely ruled out. Further studies are required to elucidate the actual acoustic power distribution of the *in vivo* rat skull. The use of low acoustic energy and duty cycle is not likely to elevate the tissue temperature and excluded the possibility of confounding the metabolic activities.

The geometry of the acoustic focus, defined by FWHM of the acoustic power distribution, was measured as a cigar-shape (6.5 mm in diameter, 24 mm in length) from skull-free calibration.[10] However, the actual modulated area, as detected by FDG-PET, was much smaller than the size of the focal dimension in both the transversal and the longitudinal directions, while there was no statistically significant hemispheric difference observed superior and inferior to the sonication center (i.e., approximate length in 6 mm along the sonication trajectory including sonication center). This highly localized nature of neuromodulation might contribute to the statistical insignificances in VOI analysis from larger brain volumes (e.g., entire hemisphere, larger spherical diameter) due to partial volume effects. Increasing sample size, as a subject for future research, will help to improve the statistical outcome. The potential distortion of the acoustic field distribution, due to the transcranial application of the FUS, might have contributed to the decreased site of modulation compared to the size of the focus. In addition, the actual modulatory effects may occur at higher acoustic intensities above the level of FWHM, e.g., full-width at two-thirds-maximum (FWTTM) (Ref. 54) or at higher intensity value. If this conjecture is true, it may suggest the need to revise the definition of the acoustic focus for the functional neuromodulation. According to the recent study on computerized simulation of the acoustic intensity distribution inside the closed rat skull by Younan *et al.*,[53] acoustic reverberations could occur inside the skull, which can significantly dilate the size of the focus in and around the skull near the sonication target. Our finding is congruent with their findings, since the actual neuromodulatory effect might take place at the concentrated region rather than the larger focal region conventionally defined by the FWHM of acoustic power distribution around the focal center. Further studies on measuring action potentials of *ex vivo* brain tissue samples, e.g., using patch-clamp,[14] which can provide the accurate area of neurons activated by FUS, or the use of high-resolution blood-oxygenation-level-dependent fMRI, may shed light on the detailed relationship between the acoustic field distribution and the spatial extent of functional neuromodulation.

In this study, a prolonged total sonication time (40 min) was adopted to increase the chances of detecting FUS-mediated changes in glucose metabolic activity during the FDG-uptake period. The sonication applied after the FDG injection could only reflect the "foot print" of ongoing FUS-mediated neuronal activity during the uptake of FDG. Therefore, the effects after the completion of sonication, i.e., post-FUS-mediated neuroactivity, could not be probed. To investigate the temporal dynamics of post-FUS-mediated neuroactivity, the sonication should be given prior to the FDG injection, and subsequent acquisition and analysis of PET imaging can be conducted.[10] The time scale of the neuromodulatory effect on glucose metabolism is dependent on many other factors such as exposure duration of sonication as well as the choice of sonication parameters, and requires future investigations.

Some may argue about excitatory effect of the sonication parameters (0.5 ms TBD, 1 kHz PRF, 300 ms SD, 3 W/cm^2 I_{spta}), used in this study. To confirm the excitatory effect of the prescribed sonication parameters, the additional experiment on determining threshold acoustic intensity for eliciting motor function (tail movement) in rats ($n = 9$, wright = 277 $\pm$ 21 g) was conducted. Based on the procedure described in Ref. 13, the elicited tail movement was recorded. The resulting threshold acoustic intensity was 3.09 $\pm$ 0.6 W/cm^2 I_{spta}. Considering extended sonication exposure (40 min) in this study compared to the previous study[13] ($\sim$10 s), the chances of evoking neural excitation with the prescribed sonication parameters are getting increased. According to the previous studies on the suppressive effect of the FUS sonication,[10,36] the FUS-induced suppressive neuromodulation seems to occur at a lower acoustic intensity with a lower duty cycle, i.e., 130 mW/cm^2 I_{spta} (Ref. 36) or 165 mW/cm^2 I_{spta} (Ref. 10) with 5% duty cycle.

Atlas-based group analysis, which utilizes the normalization of each individual rat's neuroanatomy to standardized single coordinates,[27,28] can be adopted as an alternative to VOI analysis used in this study. Group analysis based on the image-normalization has several advantages over VOI analysis. It does not require a prior hypothesis (i.e., definition of VOI), which enables the analysis of the entire brain volume, allowing for the detection of possible changes outside of the

specified regions. This feature would be beneficial in detecting the induced metabolic activity of areas other than the focal region owing to complexity in brain connectivity. Since atlas-based group analysis requires reproducible and accurate localization of the sonication, the positional accuracy when targeting the sonication needs to be improved. There were inevitable variations in positioning the focal point to the target anatomy by visual guidance based on external anatomical landmarks alone. By adopting more sophisticated localization methods, such as a real-time optical tracking system based on preoperative anatomical images,[13] the positional accuracy could be enhanced to less than 2 mm.

As for the subjects for future investigation, it is possible to utilize molecular probes for PET imaging to probe for different modes of functional neuromodulation other than glucose metabolism affected by FUS. For example, PET radiotracers labeled to have affinity to a specific neurotransmission pathway, e.g., dopamine (DA), serotonin (5-HT), and gamma-aminobutyric acid (GABA),[55–57] can be adopted. In addition, studies involving the sonication of large animals (such as, pigs or sheep) will be conducive for group analysis based on anatomical normalization, since more structural information and tissue contrast will be available for image-registration and normalization.

Various neurological and psychiatric disorders (e.g., dementia,[58] epilepsy,[59] Parkinson's disease,[60] obsessive compulsory disorder,[61] depression[62]) are known to be related to aberrant local glucose metabolic activity in the brain. Thus, the modulatory effect of FUS in brain glucose metabolism may provide several potential clinical applications. In addition to the excitatory effect of FUS on the brain confirmed in this study, FUS also has suppressive effects on the neural excitability.[10,36] This bimodal (i.e., excitatory or suppressive) modulatory property of the FUS may confer further clinical potentials, and its efficacy in modifying the local brain glucose metabolism requires further investigation.

ACKNOWLEDGMENTS

This work was supported by grants from the National Institutes of Health (R21 NS074124 to Yoo), UNIST funds (To Yoo), the National Research Foundation of Korea (Korean Ministry of Education, Science and Technology, 2010-0027294 to Kim), and the Korea Institute of Science and Technology Institutional Program (2E23031 to Yoo).

[a]Author to whom correspondence should be addressed. Electronic mail: yoo@bwh.harvard.edu; Telephone: 617-732-9464.

[1]P. P. Lele, "A simple method for production of trackless focal lesions with focused ultrasound: Physical factors," J. Physiol. **160**, 494–512 (1962).
[2]G. ter Haar, "Therapeutic applications of ultrasound," Prog. Biophys. Mol. Biol. **93**, 111–129 (2007).
[3]F. A. Jolesz, "MRI-guided focused ultrasound surgery," Annu. Rev. Med. **60**, 417–430 (2009).
[4]F. Wu, Z. B. Wang, H. Zhu, W. Z. Chen, J. Z. Zou, J. Bai, K. Q. Li, C. B. Jin, F. L. Xie, and H. B. Su, "Feasibility of US-guided high-intensity focused ultrasound treatment in patients with advanced pancreatic cancer: Initial experience," Radiology **236**, 1034–1040 (2005).
[5]K. Hynynen and F. A. Jolesz, "Demonstration of potential noninvasive ultrasound brain therapy through an intact skull," Ultrasound Med. Biol. **24**, 275–283 (1998).
[6]W. D. O'Brien, Jr., "Ultrasound-biophysics mechanisms," Prog. Biophys. Mol. Biol. **93**, 212–255 (2007).
[7]N. McDannold, G. T. Clement, P. Black, F. Jolesz, and K. Hynynen, "Transcranial magnetic resonance imaging-guided focused ultrasound surgery of brain tumors: Initial findings in 3 patients," Neurosurgery **66**, 323–332 (2010).
[8]E. Martin, D. Jeanmonod, A. Morel, E. Zadicario, and B. Werner, "High-intensity focused ultrasound for noninvasive functional neurosurgery," Ann. Neurol. **66**, 858–861 (2009).
[9]K. Hynynen, N. McDannold, N. A. Sheikov, F. A. Jolesz, and N. Vykhodtseva, "Local and reversible blood–brain barrier disruption by noninvasive focused ultrasound at frequencies suitable for trans-skull sonications," Neuroimage **24**, 12–20 (2005).
[10]S. S. Yoo, A. Bystritsky, J. H. Lee, Y. Zhang, K. Fischer, B. K. Min, N. J. McDannold, A. Pascual-Leone, and F. A. Jolesz, "Focused ultrasound modulates region-specific brain activity," Neuroimage **56**, 1267–1275 (2011).
[11]Y. Tufail, A. Matyushov, N. Baldwin, M. L. Tauchmann, J. Georges, A. Yoshihiro, S. I. Tillery, and W. J. Tyler, "Transcranial pulsed ultrasound stimulates intact brain circuits," Neuron **66**, 681–694 (2010).
[12]K. E. Hoy and P. B. Fitzgerald, "Brain stimulation in psychiatry and its effects on cognition," Nat Rev. Neurol. **6**, 267–275 (2010).
[13]H. Kim, A. Chiu, S. Park, and S.-S. Yoo, "Image-guided navigation of single-element focused ultrasound transducer," Int. J. Imaging Syst. Technol. **22**, 177–184 (2012).
[14]W. J. Tyler, Y. Tufail, M. Finsterwald, M. L. Tauchmann, E. J. Olson, and C. Majestic, "Remote excitation of neuronal circuits using low-intensity, low-frequency ultrasound," PLoS ONE **3**, e3511 (2008).
[15]P. S. Yang, H. Kim, W. Lee, M. Bohlke, S. Park, T. J. Maher, and S. S. Yoo, "Transcranial focused ultrasound to the thalamus is associated with reduced extracellular GABA levels in rats," Neuropsychobiology **65**, 153–160 (2012).
[16]B.-K. Min, P. S. Yang, M. Bohlke, S. Park, D. R. Vago, T. J. Maher, and S.-S. Yoo, "Focused ultrasound modulates the level of cortical neurotransmitters: Potential as a new functional brain mapping technique," Int. J. Imaging Syst. Technol. **21**, 232–240 (2011).
[17]W. Gsell, C. De Sadeleer, Y. Marchalant, E. T. MacKenzie, P. Schumann, and F. Dauphin, "The use of cerebral blood flow as an index of neuronal activity in functional neuroimaging: Experimental and pathophysiological considerations," J. Chem. Neuroanat **20**, 215–224 (2000).
[18]NEMA, *Acoustic Output Measurement Standard for Diagnostic Ultrasound Equipment* (National Electrical Manufactures Association, Washington, DC, 2004).
[19]F. A. Duck, "Medical and non-medical protection standards for ultrasound and infrasound," Prog. Biophys. Mol. Biol. **93**, 176–191 (2007).
[20]E. T. Fonoff, J. F. Pereira, Jr., L. V. Camargo, C. S. Dale, R. L. Pagano, G. Ballester, and M. J. Teixeira, "Functional mapping of the motor cortex of the rat using transdural electrical stimulation," Behav. Brain Res. **202**, 138–141 (2009).
[21]R. L. King, J. R. Brown, W. T. Newsome, and K. B. Pauly, "Effective parameters for ultrasound-induced in vivo neurostimulation," Ultrasound Med. Biol. **39**, 312–331 (2013).
[22]Y. Wang, J. Seidel, B. M. Tsui, J. J. Vaquero, and M. G. Pomper, "Performance evaluation of the GE healthcare eXplore VISTA dual-ring small-animal PET scanner," J. Nucl. Med. **47**, 1891–1900 (2006).
[23]X. Liu, C. Comtat, C. Michel, P. Kinahan, M. Defrise, and D. Townsend, "Comparison of 3-D reconstruction with 3D-OSEM and with FORE+OSEM for PET," IEEE Trans. Med. Imaging **20**, 804–814 (2001).
[24]F. Maes, A. Collignon, D. Vandermeulen, G. Marchal, and P. Suetens, "Multimodality image registration by maximization of mutual information," IEEE Trans. Med. Imaging **16**, 187–198 (1997).
[25]H. Engel, H. Steinert, A. Buck, T. Berthold, R. A. Huch Boni, and G. K. von Schulthess, "Whole-body PET: Physiological and artifactual fluorodeoxyglucose accumulations," J. Nucl. Med. **37**, 441–446 (1996).
[26]T. E. Nichols, J. Qi, E. Asma, and R. M. Leahy, "Spatiotemporal reconstruction of list-mode PET data," IEEE Trans. Med. Imaging **21**, 396–404 (2002).
[27]J. S. Lee, S. H. Ahn, D. S. Lee, S. H. Oh, C. S. Kim, J. M. Jeong, K. S. Park, J. K. Chung, and M. C. Lee, "Voxel-based statistical analysis of cerebral glucose metabolism in the rat cortical deafness model by 3D reconstruction of brain from autoradiographic images," Eur. J. Nucl. Med. Mol. Imaging **32**, 696–701 (2005).

[28]D. J. Rubins, W. P. Melega, G. Lacan, B. Way, A. Plenevaux, A. Luxen, and S. R. Cherry, "Development and evaluation of an automated atlas-based image analysis method for microPET studies of the rat brain," NeuroImage **20**, 2100–2118 (2003).
[29]M. Harri, T. Mika, H. Jussi, O. S. Nevalainen, and H. Jarmo, "Evaluation of partial volume effect correction methods for brain positron emission tomography: Quantification and reproducibility," J. Med. Phys. **32**, 108–117 (2007).
[30]K. Shimoji, L. Ravasi, K. Schmidt, M. L. Soto-Montenegro, T. Esaki, J. Seidel, E. Jagoda, L. Sokoloff, M. V. Green, and W. C. Eckelman, "Measurement of cerebral glucose metabolic rates in the anesthetized rat by dynamic scanning with 18F-FDG, the ATLAS small animal PET scanner, and arterial blood sampling," J. Nucl. Med. **45**, 665–672 (2004).
[31]A. M. Loening and S. S. Gambhir, "AMIDE: A free software tool for multimodality medical image analysis," Mol. Imaging **2**, 131–137 (2003).
[32]Z. Walker, D. C. Costa, R. W. Walker, L. Lee, G. Livingston, E. Jaros, R. Perry, I. McKeith, and C. L. Katona, "Striatal dopamine transporter in dementia with Lewy bodies and Parkinson disease: A comparison," Neurology **62**, 1568–1572 (2004).
[33]M. I. Martic-Kehl, S. M. Ametamey, M. F. Alf, P. A. Schubiger, and M. Honer, "Impact of inherent variability and experimental parameters on the reliability of small animal PET data," EJNMMI Res. **2**, 26 (2012).
[34]H. Fukuyama, T. Hayashi, Y. Katsumi, H. Tsukada, and H. Shibasaki, "Issues in measuring glucose metabolism of rat brain using PET: The effect of Harderian glands on the frontal lobe," Neurosci. Lett. **255**, 99–102 (1998).
[35]Y. Kuge, K. Minematsu, Y. Hasegawa, T. Yamaguchi, H. Mori, H. Matsuura, N. Hashimoto, and Y. Miyake, "Positron emission tomography for quantitative determination of glucose metabolism in normal and ischemic brains in rats: An insoluble problem by the Harderian glands," J. Cereb. Blood Flow Metab. **17**, 116–120 (1997).
[36]B. K. Min, A. Bystritsky, K. I. Jung, K. Fischer, Y. Zhang, L. S. Maeng, S. I. Park, Y. A. Chung, F. A. Jolesz, and S. S. Yoo, "Focused ultrasound-mediated suppression of chemically-induced acute epileptic EEG activity," BMC Neurosci. **12**, 23 (2011).
[37]P. Fox, R. Ingham, M. S. George, H. Mayberg, J. Ingham, J. Roby, C. Martin, and P. Jerabek, "Imaging human intra-cerebral connectivity by PET during TMS," NeuroReport **8**, 2787–2791 (1997).
[38]H. R. Siebner, F. Willoch, M. Peller, C. Auer, H. Boecker, B. Conrad, and P. Bartenstein, "Imaging brain activation induced by long trains of repetitive transcranial magnetic stimulation," NeuroReport **9**, 943–948 (1998).
[39]C. R. Ries and E. Puil, "Mechanism of anesthesia revealed by shunting actions of isoflurane on thalamocortical neurons," J. Neurophysiol. **81**, 1795–1801 (1999).
[40]N. S. White and M. T. Alkire, "Impaired thalamocortical connectivity in humans during general-anesthetic-induced unconsciousness," NeuroImage **19**, 402–411 (2003).
[41]D. D. Koblin, "Urethane: Help or hindrance?," Anesth. Analg. **94**, 241–242 (2002).
[42]N. Zhang, X. H. Zhu, Y. Zhang, and W. Chen, "An fMRI study of neural interaction in large-scale cortico-thalamic visual network," Neuroimage **42**, 1110–1117 (2008).
[43]H.-K. Min, S.-C. Hwang, M. P. Marsh, I. Kim, E. Knight, B. Striemer, J. P. Felmlee, K. M. Welker, C. D. Blaha, S.-Y. Chang, K. E. Bennet, and K. H. Lee, "Deep brain stimulation induces BOLD activation in motor and non-motor networks: An fMRI comparison study of STN and EN/GPi DBS in large animals," Neuroimage **63**, 1408–1420 (2012).
[44]F.-E. Roux, D. Ibarrola, Y. Lazorthes, and I. Berry, "Chronic motor cortex stimulation for phantom limb pain: A functional magnetic resonance imaging study: Technical case report," Neurosurgery **48**, 681–688 (2001).
[45]K. Masamoto, T. Kim, M. Fukuda, P. Wang, and S.-G. Kim, "Relationship between neural, vascular, and bold signals in isoflurane-anesthetized rat somatosensory cortex," Cereb. Cortex **17**, 942–950 (2007).
[46]C. J. Kalkman, J. C. Drummond, and A. A. Ribberink, "Low concentrations of isoflurane abolish motor evoked responses to transcranial electrical stimulation during nitrous oxide/opioid anesthesia in humans," Anesth. Analg. **73**, 410–415 (1991).
[47]B. Calancie, K. J. Klose, S. Baier, and B. A. Green, "Isoflurane-induced attenuation of motor evoked potentials caused by electrical motor cortex stimulation during surgery," J. Neurosurg. **74**, 897–904 (1991).
[48]R. King, J. Brown, W. Newsome, and K. Butts Pauly, *Proceeding of the 12th International Symposium on Therapeutic Ultrasound*, Heidelberg, Germany, A-359, 109 (2012).
[49]R. A. Wahab, M. Choi, Y. Liu, V. Krauthamer, V. Zderic, and M. R. Myers, "Mechanical bioeffects of pulsed high intensity focused ultrasound on a simple neural model," Med. Phys. **39**, 4274–4283 (2012).
[50]S. A. Goss, R. L. Johnston, and F. Dunn, "Comprehensive compilation of empirical ultrasonic properties of mammalian tissues," J. Acoust. Soc. Am. **64**, 423–457 (1978).
[51]M. M. Elwassif, Q. Kong, M. Vazquez, and M. Bikson, "Bio-heat transfer model of deep brain stimulation-induced temperature changes," J. Neural. Eng. **3**, 306–315 (2006).
[52]H. Kim, S. J. Taghados, K. Fischer, L. S. Maeng, S. Park, and S. S. Yoo, "Noninvasive transcranial stimulation of rat abducens nerve by focused ultrasound," Ultrasound Med. Biol. **38**, 1568–1575 (2012).
[53]Y. Younan, T. Deffieux, B. Larrat, A. Souilah, M. Fink, J.-F. Aubry, and M. Tanter, *Proceeding of the 12th International Symposium on Therapeutic Ultrasound*, Heidelberg, Germany, A-374, 106 (2012).
[54]A. M. Ababneh, C. C. Large, and S. Georghiou, "Solvation of nucleosides in aqueous mixtures of organic solvents: Relevance to DNA open base-pairs," Biophys. J. **85**, 1111–1127 (2003).
[55]A. L. Brownell, E. Livni, W. Galpern, and O. Isacson, "In vivo PET imaging in rat of dopamine terminals reveals functional neural transplants," Ann. Neurol. **43**, 387–390 (1998).
[56]M. Suehiro, U. Scheffel, R. F. Dannals, H. T. Ravert, G. A. Ricaurte, and H. N. Wagner, Jr., "A PET radiotracer for studying serotonin uptake sites: Carbon-11-McN-5652Z," J. Nucl. Med. **34**, 120–127 (1993).
[57]A. L. Malizia, V. J. Cunningham, C. J. Bell, P. F. Liddle, T. Jones, and D. J. Nutt, "Decreased brain GABA(A)-benzodiazepine receptor binding in panic disorder: Preliminary results from a quantitative pet study," Arch. Gen. Psychiatry **55**, 715–720 (1998).
[58]K. Ishii, "Clinical application of positron emission tomography for diagnosis of dementia," Ann Nucl. Med. **16**, 515–525 (2002).
[59]J. Engel, Jr., D. E. Kuhl, and M. E. Phelps, "Patterns of human local cerebral glucose metabolism during epileptic seizures," Science **218**, 64–66 (1982).
[60]D. Rougemont, J. C. Baron, P. Collard, P. Bustany, D. Comar, and Y. Agid, "Local cerebral glucose utilisation in treated and untreated patients with Parkinson's disease," J. Neurol., Neurosurg. Psychiatry **47**, 824–830 (1984).
[61]C. Benkelfat, T. E. Nordahl, W. E. Semple, A. C. King, D. L. Murphy, and R. M. Cohen, "Local cerebral glucose metabolic rates in obsessive-compulsive disorder. Patients treated with clomipramine," Arch. Gen. Psychiatry **47**, 840–848 (1990).
[62]S. H. Kennedy, K. R. Evans, S. Kruger, H. S. Mayberg, J. H. Meyer, S. McCann, A. I. Arifuzzman, S. Houle, and F. J. Vaccarino, "Changes in regional brain glucose metabolism measured with positron emission tomography after paroxetine treatment of major depression," Am. J. Psychiatry **158**, 899–905 (2001).